

Simulation and Measurement of Human Respiration and Heartbeat with Millimeter-Wave Radar

Yuxuan Hu, Zhaoyang Xia, Feng Xu

Key lab of Electromagnetic Wave Information Science, Fudan University

Abstract

This paper establishes a multi-scattering point chest wall motion model by combining the human respiration signal (RS) and HS (HS) measured by radar. An algorithmic process is designed based on the model to accurately separate the human respiration and heartbeat motion. Firstly, a human maximum motion velocity constraint method is proposed to correct human chest wall tracking, determine the radial position of the chest wall relative to the radar, and extract the phase signal corresponding to the chest wall motion. Then an improved time-difference method is proposed to suppress the interference of RS harmonics on HS and the interference of low-frequency noise on RS. Finally, an adaptive Gaussian weighting filter is designed to extract the RS with less distortion from the phase signal. A low-order finite-length unit impulse response (FIR) filter is used to extract the HS with less distortion from the phase signal. To verify the effectiveness of the proposed algorithm, simulating the process of measuring the RS and HS of the chest wall motion model by radar. The simulation results show that, ideally, the radar measurement results of the RS and HS are less distorted relative to the actual values. In addition, we used a millimeter wave experimental radar system in the 60 GHz band to measure the respiration rate (RR) and HR (HR) of two subjects. The experimental results showed that the measured RR and HR correlated well with the actual values. The quantitative analysis of simulation results and experimental results show that the proposed method can achieve accurate and robust measurement of respiratory and HS.

Index Terms — millimeter-wave radar, measurement of respiration and heartbeat, chest wall motion model, phase signal processing, adaptive Gaussian weighting

I. Introduction

In recent years, people have become increasingly concerned about health issues. Vital signs such as respiration and heartbeat directly reflect people's health status. Therefore, the measurement of respiration and heartbeat has important practical significance. Respiration and heartbeat measurements are widely used and can be applied to human health monitoring in the smart home [1], intelligent cockpit [2], and intelligent medical [3] scenarios, especially for elderly and infant groups [4] [5] and health condition monitoring of chronic disease patients [6].

Current widely used techniques for respiration and heartbeat measurement rely on contact sensors [7]. Measurement methods include electrocardiogram (ECG) obtained using Electrocardiography [8], photoplethysmogram (PPG) obtained using Photoplethysmography [9], air properties of human inhalation and exhalation such as carbon dioxide concentration [10], humidity [11], and temperature [12], and also chest wall mechanical displacement measurements [13]. However, contact sensors are cumbersome to wear procedures, inconvenient to move, uncomfortable to wear for long periods, and difficult to achieve continuous measurements around the clock, and non-contact sensors can overcome these drawbacks to achieve senseless and flexible all-day vital sign monitoring.

There are several methods used for non-contact human respiration and heartbeat measurements. The main non-radar based methods include visible light images [14] [15], thermal images [16], acoustic waves [17] and wireless networks (Wi-Fi) [18], and radar-based methods include continuous wave Doppler radar [19] [20], pulsed ultra-wideband radar [21], frequency modulated continuous wave radar [22] -[27], etc. However, visible and thermal image-based methods are susceptible to light, smoke, obscuration, and temperature interference and risk privacy leakage. Acoustic wave-based methods are susceptible to propagation speed and diffraction. Non-wideband wireless communication signals such as Wi-Fi have low distance resolution, and Doppler radar methods have no distance resolution. So these two methods are poorly resistant to interference. In contrast, pulsed ultra-wideband and millimeter wave radars enable non-contact, privacy-free,

long-range, interference-resistant breathing and heartbeat measurement. However, pulsed ultra-wideband radar is more costly and limited by power density [7]. In contrast, large bandwidth millimeter wave radar has the advantages of high range resolution, high Doppler resolution, lower cost, and is not limited by power density. And with the wide application of millimeter-wave radar in civil applications, some studies based on FM continuous-wave millimeter-wave radar for respiration and heartbeat measurements already exist.

Xiong proposed the parametric demodulation (PD) method [22] to extract RS and HS directly from the baseband signal. However, achieving accurate respiration and heartbeat measurements is difficult when the respiration harmonics interfere with the heartbeat or when the RR is adjacent to the heartbeat. The more commonly used method for respiration and heartbeat measurement is first to track the chest wall position, extract the time-varying phase signal corresponding to the chest wall motion, and then extract RS and HS. The key to realizing respiration and heartbeat measurement in this method is how to separate the respiration and heartbeat motions accurately. The current plans are mainly divided into frequency-domain methods and time-domain methods.

The main frequency domain-based methods are filters [23-25]. Hanifi and Zhang proposed using band-pass filters to extract RS and HS [23-24]. However, since the frequencies of RS and HS vary within a specific interval, a fixed bandwidth of the filter will result in irrelevant signals falling within the passband or attenuating relevant signals. Also, Lv proposed the method of extracting the RS and HS spectrum using matched filters [25]. However, it is challenging to extract RS and HS accurately when the noise frequency is similar to the frequencies of respiration and heartbeat.

Regarding the time-domain method, Mi used a modified Wavelet Transform (WT) method to extract the HS [26], wavelet decomposition followed by reconstruction, and then peak detection method to estimate RR and HR.

Zhang proposed to extract the HS using the Wigner-Ville Distribution (WVD) [27]. Fang and Wang used Ensemble Empirical Mode Decomposition (EEMD) [28] and Multivariate Empirical Mode Decomposition (MEMD) [29] to extract the Intrinsic Mode Function (IMF). Then the RR and HR was obtained by correlating the IMF with the frequency range of the respiration and heartbeat. Li used Singular Value Decomposition (SVD) to process the phase signal and then, based on Fast Fourier Transform (FFT) and Hilbert-Huang Transform (HHT), transformed it into RS and HS [30]. Zhao proposed the Synchro Squeezing Transform (SST) method to extract RS and HS [31]. Tu reconstructed the respiration time-domain signal by extracting the spectrum of the RS from the received signal and subtracting the RS in the time domain to eliminate the effect of respiration harmonics on the HS [32]. Xiong proposed to make a second-order time difference on the phase signal to eliminate the effect of respiration harmonics on HR estimation [33], which facilitates the extraction of more accurate HS. But the second-order time difference processing leads to the disappearance of the heartbeat spectrum.

The time-frequency method can accurately measure respiration and heartbeat provided that it can accurately track the chest wall position and that there is little influence between the spectrum of low-frequency noise, RS and HS. However, during realistic measurements, the tracking of chest wall position is susceptible to shifts or jumps due to radar system noise and multipath noise. Due to the influence of low-frequency clutter, the RS is not easily extracted accurately. Since the HS is weak, detecting when the clutter interferes with it is not easy, especially when the respiration harmonics affect the HS. Existing studies fail to solve these problems well. Therefore, in this paper, we combine the actual human respiration and heartbeat motion, establish a human chest wall motion model, and study the accurate tracking method of the human chest wall, as well as the demixing method of RS and HS and noise signal. Finally, achieve accurate measurement of human breathing and heartbeat motion by radar.

Human chest wall motion models help to assess the accuracy of measurements of respiration and heartbeat. There have been several studies on human chest wall motion models. Xiong used trigonometric signals [22] to represent respiratory and HS. Ambarini and Xia used a single point to represent the chest wall, an ECG signal [35], a triangular pulse signal and a triangular function signal [34] to represent the HS. Lu used a metal reflector with a fixed vibration frequency to simulate chest wall motion [36]. However, the simulation of chest wall motion by the above methods is inaccurate. The respiratory frequency of a healthy human body at rest is 12-20 beats per minute (BPM), the HR is 60-100 BPM, and the frequency and amplitude vary with time. The motion frequency and amplitude of the simulated chest wall in the above method are too idealized and do not match the human physiological characteristics. Besides, it is not reasonable to use the ECG signal as the HS because the measurement frame rate of the radar is low, and it cannot acquire the same resolution as the ECG.

In general, existing studies of chest wall motion models have the following problems.

1) The chest wall is insufficient to characterize the real chest wall when it is regarded as a single point.

2) The simulation of RS and HS differs greatly from the real situation.

Existing studies on the measurement of RS and HS face the following challenges.

1) Random body movement (RBM) causes the chest wall position to be tracked incorrectly.

2) The spectrum of low-frequency noise, RS, and HS interact with each other, which makes it difficult to extract RS and HS accurately.

This paper proposes an accurate extraction method for human RS, and HS by combining simulation and experimental research to address the above problems.

The contributions of this paper are as follows.

1) Transforming the radar-measured human RS into the modeled respiratory motion by building a multi-scattering point columnar motion model closer to the real human chest wall motion. The radar-measured HS when holding the breath is transformed into the heartbeat motion of the model. The model can relate the ideal to real human chest wall motion and is used to evaluate the accuracy of the proposed method for respiration and heartbeat measurements.

2) Propose a maximum human motion velocity constraint algorithm to accurately track chest wall radial position.

3) Propose a phase signal processing method combining time difference and outlier cancellation, which can suppress the interference of low-frequency noise on RS and respiratory harmonics on HS.

4) The adaptive Gaussian smoothing filter and FIR band-pass filter are proposed to extract the RS and HS accurately and then obtain the RR and HR.

The remaining sections of this paper are organized as follows. Section II establishes the human chest wall motion model. Section III presents the extraction method of respiration and heartbeat. In Section IV, we perform the evaluation of simulation and experiments. In Section V, we discuss the residual issues and future work.

II. Chest wall motion model

A. Radar signal model

In this paper, a linear frequency modulated continuous wave (LFMCW) millimeter wave radar is used, whose transmit signal can be expressed as [37]

$$S_{tx}(t) = A_T \exp[-j \cdot (2\pi f_0 t + \pi K_s t^2)] \#(1)$$

Where A_T denotes the transmit signal amplitude, f_0 is the transmit signal frequency, and K_s is the FM slope.

The echo signal obtained after reflection from a micro-motion point target is

$$S_{rx}(t) = A_R \exp\{-j \cdot [2\pi f_0(t - \tau) + \pi K_s(t - \tau)^2 + 2\pi f_d(t - \tau)]\} \#(2)$$

where A_R denotes the transmit signal amplitude, $\tau = 2R_0/c$ is the time elapsed from transmitting to receiving the signal, and $f_d = 2v_r/\lambda$ is the Doppler shift. R_0 is the distance between the radar and the human target to be measured, c is the speed of light, v_r is the radial velocity of the human body relative to the transmit signal, and λ is the wavelength of the transmit signal.

The phase of the IF signal is the phase difference between the transmitted signal and the received signal, and the IF signal obtained by chest wall reflection can be expressed as

$$S_{if}(t) = A_T A_R \exp\{j \cdot [\varphi_{tx}(t) - \varphi_{rx}(t)]\} \#(3)$$

Where $\varphi_{tx}(t)$ and $\varphi_{rx}(t)$ are the phase signals of the transmitted signal and the received signal, respectively.

According to Geometrical Theory of Diffraction (GTD), when the incident wave wavelength is much smaller than the target size, the backscattered field of the target can be represented as a superposition of a series of independent scattering centers [38]. Therefore, in this paper, the human chest wall is modeled as N scattering points, and the distance of each scattering point relative to the radar is R_i , $i = 1, 2, \dots, N$. The time elapsed from transmitting to receiving the signal is $\tau_i = 2R_i/c$. The Doppler shift is $f_{di} = 2v_{ri}/\lambda$. The average inter-frame radial velocity of the chest wall relative to the radar can be expressed as

$$v_{ri}(t) = \frac{[R_i(t) - R_i(t - T_f)]}{T_f} \#(4)$$

T_f denotes the frame period.

The phase of the IF signal is the phase difference between the transmitted signal and the received signal, and the phase difference obtained by the reflection of the i th thorax point can be expressed as

$$\varphi_{if}(t, i) = \varphi_{tx}(t, i) - \varphi_{rx}(t, i) = 2\pi f_0 \tau_i + 2\pi f_{di} \tau_i - \pi K_s \tau_i^2 + 2\pi K_s \tau_i t - 2\pi f_{di} t \#(5)$$

Since τ_i is small, the effect of $\pi K_s \tau_i^2$ term on the phase signal $\varphi_{if}(t, i)$ can be neglected, and since f_{di} is much smaller than f_0 , the effect of $2\pi f_{di} \tau_i$ can be neglected. The phase signal can be approximated as

$$\varphi_{if}(t, i) = 2\pi f_0 \tau_i + 2\pi K_s \tau_i t - 2\pi f_{di} t \#(6)$$

Where $K_s \tau_i$ denotes the frequency change of the signal f_{τ_i} in τ_i time, and $K_s \tau_i$ is only related to the sampling point per FM cycle (i.e., fast time). Since each FM cycle is very short, the change of f_{di} in one FM cycle can be neglected and is only related to the FM cycle time (i.e., slow time). Assuming that the bandwidth of the FM continuous wave is B and the FM period is T_s , there is $K_s = B/T_s = f_{\tau_i}/\tau_i$, and the target distance can be expressed as [37]

$$R_i = \frac{c T_s f_{\tau_i}}{2B} \#(7)$$

The IF signal corresponding to the i -th point can be expressed as

$$S_{if}(t, i) = A_{T_i} A_{R_i} \exp[j \cdot \varphi_{if}(t, i)] \#(8)$$

Then the signal superposition of N points can be expressed as

$$S_{if}(t) = \sum_{i=1}^N A_{T_i} A_{R_i} \exp[j \cdot \varphi_{if}(t, i)] = B(t) \cdot \exp[j \cdot \varphi_{IF}(t)] \#(9)$$

For an FM period of IF signal sampling, if there are I_{adc} sampling points and the sampling period is T_{adc} , the discrete form of the IF signal can be obtained as

$$S_{if}(j) = B(j) \cdot \exp[j \cdot \varphi_{if}(j)] \#(10)$$

Where $j = 1, 2, \dots, N_{adc}$ and $B(j)$ is the amplitude of the IF signal.

Fast Fourier transform of discrete IF signal $S_{if}(j)$ can get the target distance-dependent IF signal spectrum $f_{if}(j)$, which is the distance-amplitude distribution map within the measurable range of the radar. The maximum amplitude detection is done on the distance-amplitude distribution map to get the distance index j_{trgt} of a single target. Then the target point phase is extracted as

$$\varphi_{trgt}(m) = j \cdot \varphi_{IF}(j_{trgt}) \#(11)$$

where m denotes the frame index.

B. Chest wall motion model

According to the physiological structure of the human chest wall, we consider the chest wall as a cylindrical surface with a radius of R [39], and the area of the column surface is about $1.5 \times 10^3 \text{cm}^2$. According to GTD, the human chest cavity is represented as multiple scattering points. In the three-dimensional right-angle coordinate system shown in Fig. 1(a), the human chest wall is represented as nine scattering points, i.e., $N = 9$ in Section II, Part A. The scattering points are defined as $S_0, S_1, S_2, S_3, S_4, S_5, S_6, S_7, S_8$ in order. the top view of the simulated human chest wall is shown in Fig. 1(b). The center of the cylinder is O , the radius of the cylinder R is 0.0125m, and the coordinates and vibration coefficients of the nine scattering points on the cylinder are set as shown in Table 1. Let the nine scattering points move along the X-axis, and the motion intensity gradually decays outward from the center of the column surface to form a chest wall motion model. The motion signals of the nine scattering points can be expressed as

$$S_i = \begin{cases} k_0 \cdot B(x) & i = 0 \\ k_1 \cdot B(x) & i = 1, 3, 5, 7 \\ k_2 \cdot B(x) & i = 2, 4, 6, 8 \end{cases} \#(12)$$

Where $B(x)$ is the motion signal at the center point of the chest wall, k_0, k_1 and k_2 are the vibration coefficients, and k_0, k_1

and k_2 are set to 1, 1/2 和 1/3, respectively, according to the physiological structure of the human chest wall.

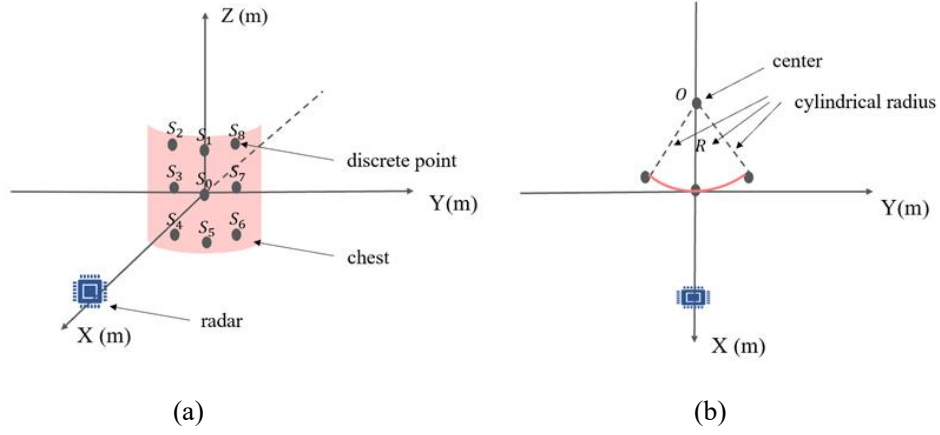


Fig. 1 (a) shows a three-dimensional view of the simulated chest wall structure; (b) shows a top view of the simulated chest wall structure.

Table 1 Radius of the chest wall model and the coordinates of each scattering point

Parameters	Values(m)	Coefficient
S_0	(0, 0, 0)	k_0
S_1	(0, 0, 0.01)	k_1
S_2	(-0.005, -0.01, 0.01)	k_2
S_3	(-0.005, -0.01, 0)	k_1
S_4	(-0.005, -0.01, -0.01)	k_2
S_5	(0, 0, -0.01)	k_1
S_6	(-0.005, 0.01, 0.01)	k_2
S_7	(-0.005, 0.01, 0)	k_1
S_8	(-0.005, 0.01, -0.01)	k_2

The movement frequency and amplitude of human respiration and heartbeat are not fixed, so they cannot be represented by a function of fixed frequency and amplitude. We propose converting the radar-measured HS into modeled respiration and heartbeat. Let A subject sit with the chest wall facing the radar at 0.5 m from the radar, and the radar was used to detect the chest wall motion of the volunteer. Section IV-A will describe detailed radar configuration information and signal processing process. The radar frame rate was 20 Hz/s, and the respiratory and heartbeat movements were collected as scattered point data. According to Section II, Part A can obtain the noise-laden phase signal representing the chest wall motion

$$\phi_i = b_{i0} + h_i + N_0 \# (13)$$

Where b_{i0} , h_i and N_0 denote the phase signals of respiration, heartbeat and noise, respectively. $i \in [1, N]$ denotes N scattering points. Smoothing filtering can eliminate the noise and HS, and the RS b_{i0} can be extracted. However, since smoothing filtering causes the signal amplitude to be attenuated, the respiration phase signal b_{i0} amplitude needs to be expanded

$$b_i = b_{i0} \cdot A_B \# (14)$$

Since the HS is weak and susceptible to respiratory harmonics, a breath-holding method is used to measure the phase signal of chest wall motion that contains only heartbeat motion and noise

$$\phi_i = h_i + N_0 \# (15)$$

After the denoising process, the heartbeat phase motion h_i is obtained, and the heartbeat phase signal without the effect of respiratory motion can better characterize the heartbeat motion. Then the respiratory phase signal b_i and the heartbeat phase

signal h_i are transformed into the respiratory and heartbeat motions of the simulated chest wall. The relationship between motion amplitude and phase is

$$\Delta R = \frac{\lambda}{4\pi} \Delta \phi_b \#(16)$$

Therefore, the phase signal needs to be transformed into a phase difference signal and a motion signal. The phase signals b_i and h_i can be transformed into respiratory motion displacement ΔB_i and heartbeat motion displacement ΔH_i , respectively

$$\Delta H_{i+1} = \frac{\lambda}{4\pi} (h_{i+1} - h_i) \#(17)$$

$$\Delta B_{i+1} = \frac{\lambda}{4\pi} (b_{i+1} - b_i) \#(18)$$

Let the initial positions H_1 and B_1 of the respiratory and HS be 0. Then the respiratory and HS can be expressed as

$$H_{i+1} = H_i + \Delta H_{i+1} \#(19)$$

$$B_{i+1} = B_i + \Delta B_{i+1} \#(20)$$

The chest wall motion $B(x)$ is the time domain summation of H_i and B_i . In addition, to make the simulation close to the real experiment, it is necessary to add white noise N_0 to the signals H_i and B_i to simulate the environmental noise

$$B(x) = H_i + B_i + N_0 \#(21)$$

By setting $B(x)$ to the chest wall motion at each scattering point according to Eq. (12), the simulated chest wall motion signal is obtained, as shown in Fig. 2. Fig. 2(a), Fig. 2(c), and Fig. 2(e) show the respiratory motion signal, heartbeat motion signal, and chest wall motion signal of the chest wall motion model, respectively. Fig. 2(b), Fig. 2(d), and Fig. 2(f) show the spectrum of respiratory motion signal, the spectrum of heartbeat motion signal, and the spectrum of chest wall motion signal of the chest wall motion model, respectively.

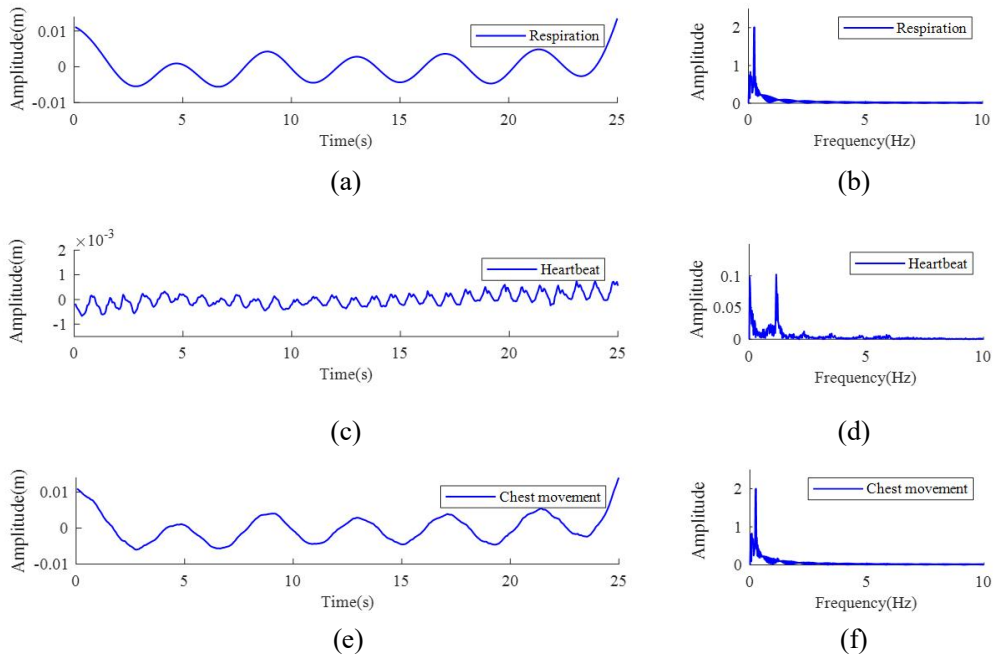


Fig. 2 (a) shows the respiratory motion signal of the exercising chest wall model; (b) shows the spectrum of the respiratory motion signal; (c) shows the heartbeat motion signal of the exercising chest wall model; (d) shows the spectrum of the heartbeat motion signal; (e) shows the chest wall motion signal of the exercising chest wall model; (f) shows the spectrum of the chest wall motion signal.

III Methods

A. Extraction and pre-processing of chest wall motion signals

First, the 1-D range profile is calculated for each frame in the measurement area based on the chest wall motion model.

Then the maximum amplitude detection of the 1-D range profile is done to estimate the radial position of the human chest wall relative to the radar. The 1-D distance image is shown in Fig. 3.

Due to environmental noise and body jitter, distance detection may have errors, and this paper proposes a human motion constraint algorithm to correct the distance estimation errors. Setting the maximum velocity of the human chest wall motion as v_{\max} , the maximum span between frames of the chest wall distance index can be determined as

$$I_{\max} = \frac{v_{\max} T_f}{d_{\text{res}}} \#(22)$$

Determine whether the distance index needs to be corrected by judging whether the span of the distance index between the current frame and the previous frame exceeds the maximum distance index span. Calculate the distance index span $d^* = |d_n - d_{n-1}|$, and determine the distance index value by judging the relationship between d^* and I_{\max}

$$d_n = \begin{cases} d_{n-1} & d^* > I_{\max} \\ d_n & d^* < I_{\max} \end{cases} \quad n \in [2, N] \#(23)$$

Where d_n and d_{n-1} are the distance indexes detected in the n th and $n-1$ th frames, respectively.

However, if the distance index of the first frame is wrong, the algorithm cannot correct the subsequent distance indexes. Hence, a stable starting distance index must first be obtained before the subsequent distance index correction. As shown in Fig. 4, the distance index values before and after the algorithm constraint are compared. We can find that the distance index distribution of the corrected chest wall is more concentrated, which indicates that the position tracking is more robust after the algorithm correction.

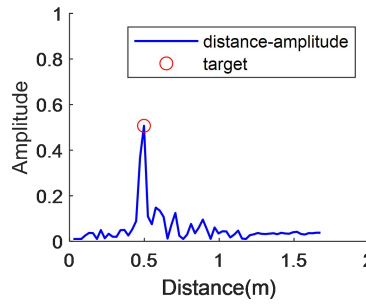
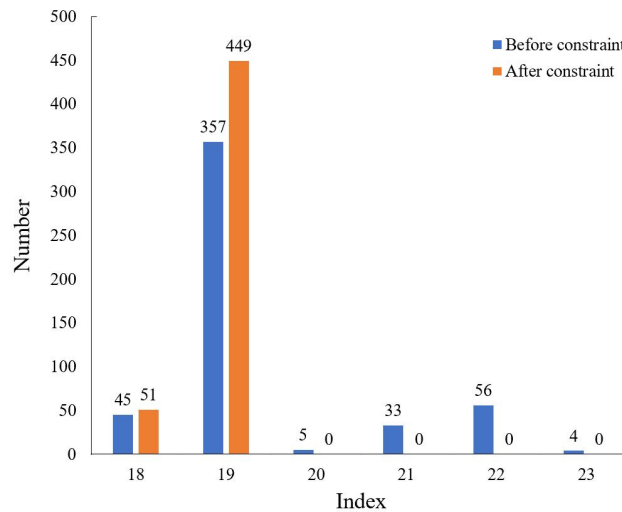


Fig. 3 1-D range profile after maximum human motion velocity



constraint.

Fig. 4 Comparison of distance indexes of 500 frames of data before and after the algorithm constraint.

According to part B of Section II, the phase signal of the current frame containing the chest wall motion can be obtained when the distance of the target point of the current frame is known. The phase jump of the signal at π leads to phase wrapped. Fig. 5(a) and Fig. 6(a) show the wrapped phase signal and its spectrum, respectively, so unwrap the wrapped phase signal first. However, due to the phase measurement noise, it is difficult to achieve perfect phase unwrapping, and the unwrapped phase signal still has large low-frequency and high-frequency noise components. Fig. 5(c)

and Fig. 6(c) show the unwrapped phase signal and its spectrum, respectively. The low-frequency components in the spectrogram are very close to the frequency band where the RS is located. The high-frequency noise almost drowns out the heartbeat frequency band information, making it difficult to accurately separate and extract RS and HS. This paper proposes an improved time-difference method to process the unwrapped phase signal and obtain the phase difference signal with suppressed low-frequency components and high-frequency noise. The unwrapped phase difference signal has burr-like outliers due to the imperfect unwrapping. Fig. 5(e) and Fig. 6(e) show the phase difference signal and its spectrum, respectively. Comparing the phase difference signal obtained from simulation Fig. 5(f) shows that the burr does not exist under ideal experimental conditions. Therefore, an outlier cancellation algorithm is designed in this paper to process the phase difference signal.

The algorithm is divided into two steps. The phase difference signal $x_n + A$ is de-meant to get x_n , and then x_n is segmented as

$$y_n = \begin{cases} k_3 \times x_n & n = 1 \text{ or } n = N, x_n \geq C_1 \\ \frac{1}{2}(x_{n-1} + x_{n+1}) & n \neq 1 \text{ and } n \neq N, |x_{n-1}| < C_1, |x_{n+1}| < C_1 \\ x_n & \text{others} \end{cases} \quad \#(24)$$

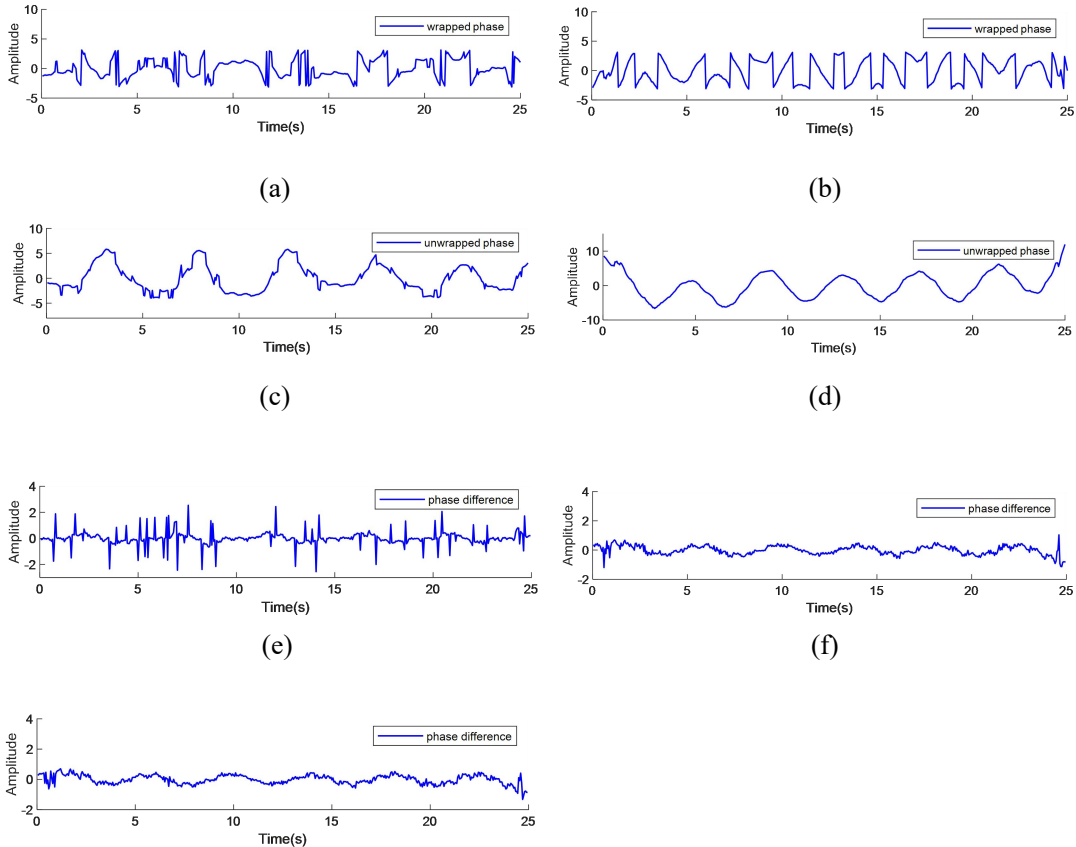
Where k_3 is the attenuation factor, and then segment y_n to obtain the phase difference signal after the second correction step

$$z_n = \begin{cases} y_{n-1} + k_4 \times \text{sgn}(y_{n+1} - y_{n-1}) & n \neq 1 \text{ and } n \neq N, |y_n - y_{n-1}| > C_2 \\ y_n & \text{others} \end{cases} \quad \#(25)$$

Where k_4 is the attenuation factor and $\text{sgn}(\ast)$ is the sign function

$$\text{sgn}(x) = \begin{cases} 1 & x > 0 \\ 0 & x = 0 \\ -1 & x < 0 \end{cases} \quad \#(26)$$

Fig. 5(g) shows the phase difference signal after outlier elimination, and Fig. 6(g) shows its spectrum. Comparing Fig. 5(e) and Fig. 6(e), we can see that the proposed outlier elimination algorithm can effectively eliminate the burr outliers and highlight the respiratory frequency, the second harmonic of respiratory frequency and the heartbeat frequency contained in the phase difference signal.



(g)

Fig. 5 (a) Wrapped phase signal; (b) Simulated wrapped phase signal; (c) unwrapped phase signal; (d) Simulated unwrapped phase signal; (e) Phase difference signal; (f) Simulated phase difference signal; (g) phase difference signal without outliers

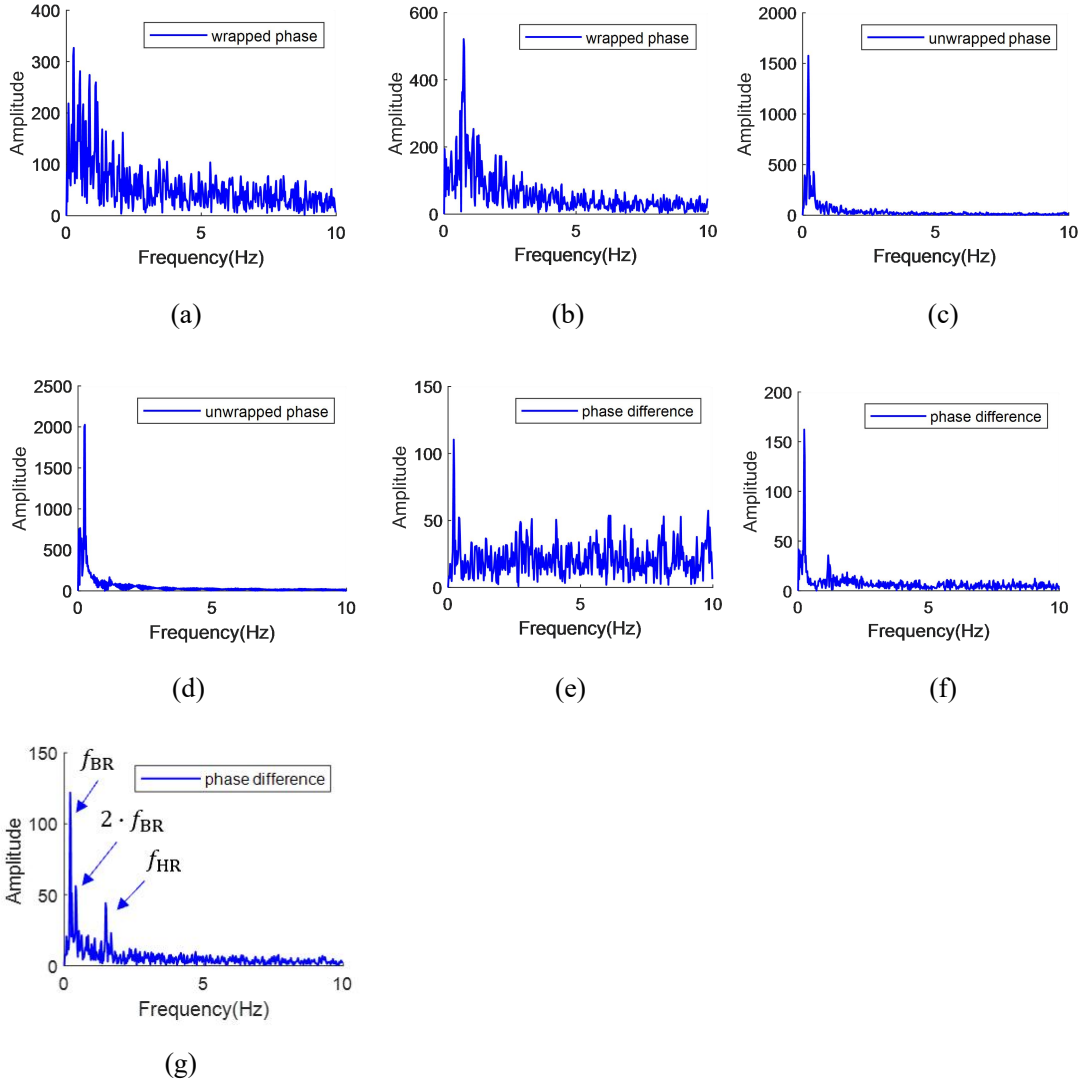


Fig. 6 (a) Spectrum of the wrapped phase signal; (b) Spectrum of the simulated wrapped phase signal; (c) Spectrum of the unwrapped phase signal; (d) Spectrum of the simulated unwrapped phase signal; (e) Spectrum of the phase difference signal; (f) Spectrum of the simulated phase difference signal; (g) Spectrum of the phase difference signal without outlier

B. RS extraction and rate calculation

The frequency of respiration is 12-20 BPM, and the frequency and bandwidth are small. Suppose a band-pass filter is used to extract the RS. In that case, it requires a small filter bandwidth, fast decay, and narrow transition band, which will lead to a large filter order, large group delay, and not easy to extract an accurate RS.

We found gaussian smoothing filtering [40] to be an effective method to restore the true RS. This method calculates the Gaussian-weighted average within each window by sliding windows to obtain the average value over time. The one-dimensional Gaussian function can be expressed as

$$f(x) = \frac{1}{\sigma\sqrt{2\pi}} e^{-(x-\mu)^2/2\sigma^2} \quad (27)$$

Assume that the sliding window length is $2n+1$ and μ and σ are the mean and standard deviation of the Gaussian function, respectively, and let $\mu = 0$. The parameter σ characterizes the width of the Gaussian filter, and the value of σ determines the degree of smoothing. When σ is too small, the extracted RS has a heartbeat component. When σ is too large, the RS is significantly distorted. Therefore, this paper proposes an adaptive Gaussian smoothing filtering method based on optimal spectral components to eliminate high-frequency noise and heartbeat components while minimizing distortion of

the RS.

Suppose the burr-free phase difference signal in Section III.A is $\hat{h}(x)$, and the Gaussian smoothing filter is $w(x, \sigma)$, then the signal of $\hat{h}(x)$ after Gaussian filtering is

$$g(x, \sigma) = \hat{h}(x) * w(x, \sigma) \quad \#(28)$$

The frequency domain form of $g(x, \sigma)$ after the Fourier transform is

$$G(f, \sigma) = \mathcal{F}[g(x, \sigma)] \quad \#(29)$$

The Respiration to Heartbeat Ratio (BHR) is defined as the ratio of respiration to heartbeat spectral energy

$$BHR = \frac{\|G_{\text{resp}}(f, \sigma)\|_2^2}{\|G_{\text{heart}}(f, \sigma)\|_2^2} \quad \#(30)$$

Where $G_{\text{resp}}(f, \sigma)$ and $G_{\text{heart}}(f, \sigma)$ are the intercepts of $G(f, \sigma)$ in the frequency band 0.2~0.4Hz and the frequency band 0.8~2Hz, respectively, and $\|*\|_2$ denotes the two-norm of $*$. Use gradient ascent to maximize the following objective function.

$$L(\sigma) = BHR = \frac{\|G_{\text{resp}}(f, \sigma)\|_2^2}{\|G_{\text{heart}}(f, \sigma)\|_2^2} \quad \#(31)$$

Where the step size λ is set to 0.01 and the initial value of σ is set to 5. The gradient ascent method will converge about 50 times to obtain a determined standard deviation σ . The optimization curve of the objective function is shown in Fig. 7. Fig. 8(a) and Fig. 8(b) show the extracted RS and their spectrograms, respectively. Fig. 8(a) Respiration B indicates the RS obtained using a Gaussian smoother, and Respiration R indicates the RS obtained using an FIR band-pass filter. The spectrum of Respiration R is shown in Fig. 8(b) with second harmonics and significant phase shift, resulting in a different RR from Respiration B.

The RR is calculated using a signal peak-seeking algorithm. The algorithm constrains the peak-seeking condition according to the respiration amplitude and frequency range. Finding all maximal values of the signal A_{max} , assuming that the number of A_{max} is L_{max} , the rate can be expressed as

$$B_{\text{rate}} = \frac{L_{\text{max}} - 1}{t} \times 60 \quad \#(32)$$

Where t is the time difference between the first and last maxima in seconds, and B_{rate} is the rate of heartbeat or respiration in BPM. The calculated rate is shown in Fig. 8.

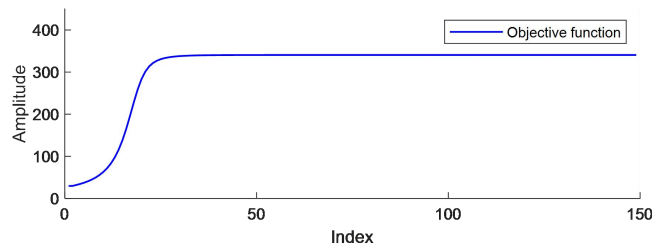


Fig. 7 Objective function optimization curve

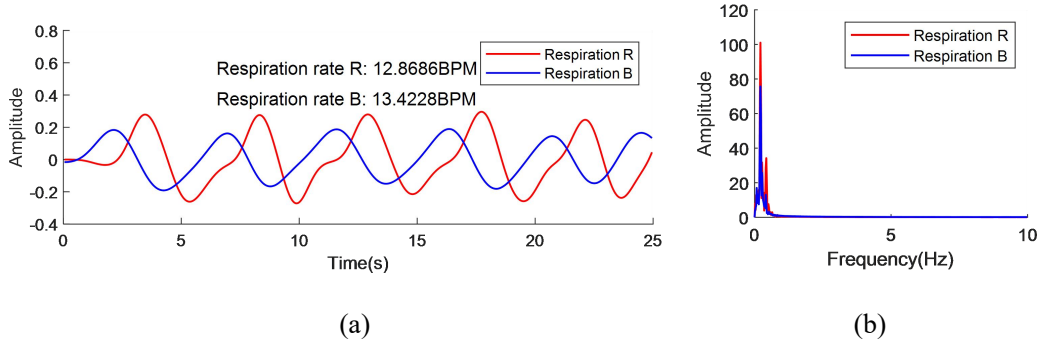


Fig. 8 Respiration B denotes the RS obtained using a Gaussian smoother, and Respiration R denotes the RS obtained using an FIR band-pass filter; (a) is the RS; (b) is the spectrogram of the RS.

B. HS extraction and rate calculation

The HR is usually 60-100 BPM. Considering that the phase frequency characteristics of the FIR filter are linear, an FIR band-pass filter is used to extract the HR signal. The heartbeat rate is calculated in the same way as breathing. The linear phase-frequency characteristics of the FIR filter lead to a group delay in the phase characteristics of the extracted HR signal, which makes the extracted HR delayed but the inter-peak interval unchanged, so the obtained HR does not change. The group delay is proportional to the filter's decay rate, so the filter's decay rate cannot be too fast.

Considering that the heartbeat frequency fluctuates within a certain range, the frequency with the largest amplitude of the heartbeat spectrum is found first, and the passband band is set to this frequency as the center frequency so that the information of the HS can be retained to the maximum extent. The extracted HS and rates are shown in Fig. 9, and Fig. 9(a) and Fig. 9(b) show the HS and their spectra, respectively. The heartbeat rate is calculated in the same way as breathing. Because of the group delay caused by the FIR filter, the time delay needs to be compensated when comparing the experiment's measured and actual heartbeat rates.

$$\tau(\omega) = -\frac{d\varphi(\omega)}{d\omega} \quad \#(33)$$

Where $\varphi(\omega)$ is the phase frequency characteristic of the filter, and since the phase frequency characteristic of FIR is linear, the time delay $\tau(\omega)$ is a constant.

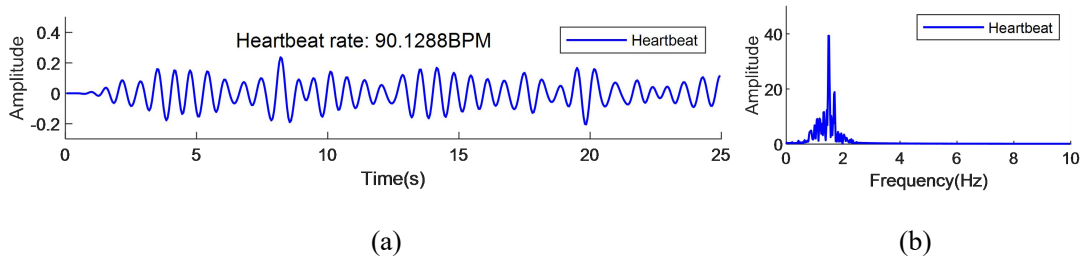


Fig. 9 (a) shows the HS; (b) shows the spectrum of the HS

IV Experimental results and analysis

This paper proposes a method for real-time acquisition of human chest wall motion data to measure respiratory heartbeat using millimeter-wave radar. To quantitatively evaluate the accuracy of the proposed method, an experimental real-time millimeter wave radar system is developed in this paper.

A. Experimental environment and equipment

The experimental scenario is shown in Fig. 10. The millimeter-wave radar development board used for the experiments was designed based on Infineon's 60 GHz band millimeter-wave radar chip. The raw ADC data was output to the computer for processing through the SPI to USB interface. The radar system parameters are shown in Table 4. A transmitting antenna and three receiving antennas are integrated into the millimeter wave radar chip, which can get three data channels. The third channel data with the largest signal-to-noise ratio is selected for subsequent processing.



Fig. 10 The experimental scenario

Table 2 Radar system parameter settings

Parameters	Definitions	Values
N_{TX}	Number of transmitting antennas	1
N_{RX}	Number of receiving antennas	3
F_{start}	Start frequency	57.5GHz
F_{stop}	Stop frequency	63.5GHz
K_s	FM slope	91.5 MHz/us
F_s	Sampling frequency	2MHz
T_{chirp}	Frequency modulation period	71.8us
T_{frame}	Frame period	50ms
λ	Wavelength	5mm
N_{chirp}	Number of chirps	2
N_{adc}	Number of receiving antennas	128
r_{res}	Range resolution	0.0256m
r_{max}	Maximum measuring range	3.2763m

B. Assessment of results

To verify the effectiveness of this algorithm, simulating the process of measuring the RS and HS of the chest wall motion model by radar. And they are then compared with the actual values. The comparison results are shown in Fig. 11. To quantify the distortion of the respiratory and heartbeat waveforms, evaluate the crest interval difference and the signal correlation coefficient. The evaluation results are shown in Table 3. The signal correlation coefficient can measure the degree of similarity between the signals [41], and the correlation coefficient range is 0 to 1. When the correlation coefficient is 1, the two signals are linearly correlated. Fig. 11(b) shows the calculation of wave crest interval difference. t_{REF1} and t_{REF2} are the moments where two adjacent wave crests of the reference waveform are located, t_{RAD1} and t_{RAD2} are the moments where two adjacent wave crests of the same period of the simulated measurement waveform are located, and the wave crest time difference t_{diff} can be expressed as

$$t_{diff} = (t_{REF2} - t_{REF1}) - (t_{RAD2} - t_{RAD1}) \quad (34)$$

The data in Table 3 show that the distortion of the RS is small, and the distortion of the HS is large. But when the filter processed the heartbeat reference signal, the distortion of the HS became smaller. So the distortion of the HS is mainly caused by the band-pass filter. This is because the amplitude-frequency response of the band-pass filter is not ideal, but this does not affect the HR calculation.

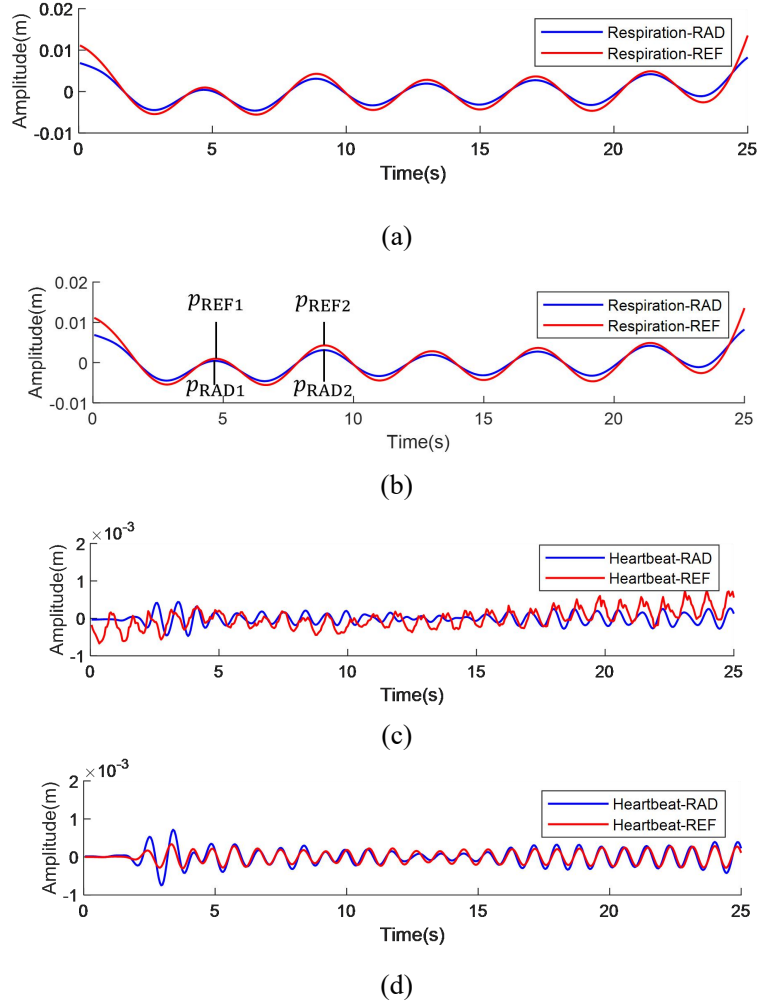


Fig. 11 Respiration-RAD is the simulated radar-measured RS, Respiration-REF is the actual RS; (a) comparison of the two RS; (b) schematic diagram of the calculation of the difference between the wave crests of the two RS; Heartbeat-RAD is the simulated radar-measured HS, and Heartbeat-REF is the actual HS; (c) is the comparison of the two HS; (d) the filter processing Heartbeat-REF and Heartbeat-RAD comparison.

Table 3 Comparison of the simulated respiration and heartbeat radar measurements

Type	MEAN/s	Mean error rate/%	SD/s	Correlation coefficient
Respiration	0.03	0.71	0.03	0.9842
Heartbeat	0.04	5.00	0.13	0.7176
Heartbeat 2	0.006	0.64	0.05	0.9337

To verify the algorithm's accuracy in measuring respiratory and HR in a real-world scenario, we recruit two healthy subjects (one male and one female, age range 22-25), with the chest wall facing the radar sitting 0.5m from the front of the radar. Chest wall motion and heartbeat were recorded with the camera and the pulse oximeter, respectively.

As shown in Fig. 12, x_{min} is the chest wall motion peak, and x_{max} is the trough. The time interval t_{RES} corresponding to the adjacent respiratory wave peak is recorded for the chest wall motion video captured by the camera. The actual RR is calculated using the algorithm in Section III.B. The HR is measured with a pulse oximeter. The accuracy of the radar measurements is then assessed by comparing the radar measurements with the actual values.

We recorded 21 respiratory wave intervals for the two subjects. A comparison of the radar measurements with the actual values is shown in Fig. 13 for two subjects coded as F and M. A comparison of the 17 HR variation curves recorded by us for the two subjects over 50 s is shown in Fig. 14.

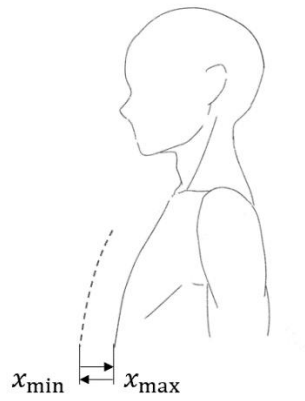


Fig. 12 Schematic diagram of the actual RR calculation of the experimental subjects

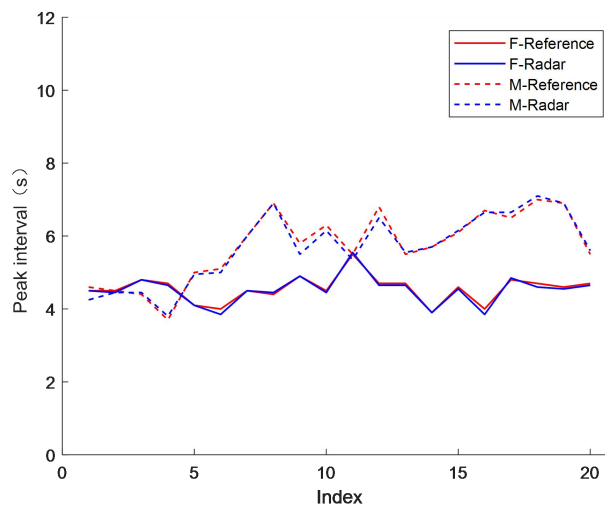


Fig. 13 Comparison of radar measurements and actual values of respiratory wave intervals of experimental subjects F and M

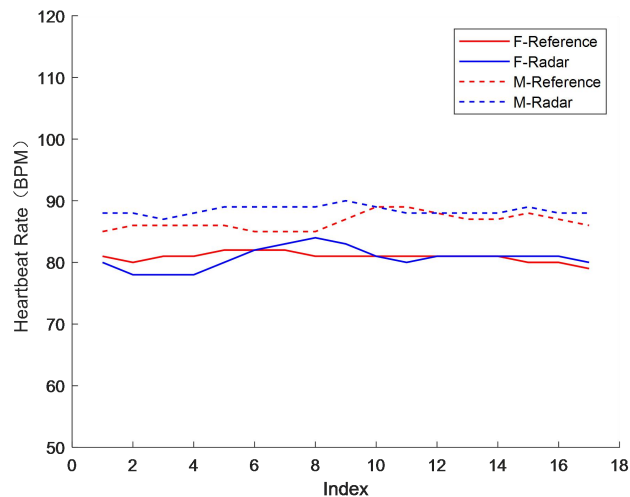


Fig. 14 Comparison of radar measurements and actual HR values of experimental subjects F and M

The article quantitatively analyzes the respiratory and heartbeat measurements, and the results of the analysis are shown in Table 4 and Table 5. The article analyzed the radar measurements of the inter-peak interval of the RS with the actual values, and the difference between the mean values was within 0.05s. The difference in the standard deviation was within 0.03s. The article also analyzes the radar measurements of the HS rate and the actual values. The difference between the mean value and the actual value is within 2 BPM, and the difference between the standard deviation is within 2 BPM. The experimental data show that the radar measurements of the human respiratory heartbeat have a small difference from

the reference value and a high accuracy rate.

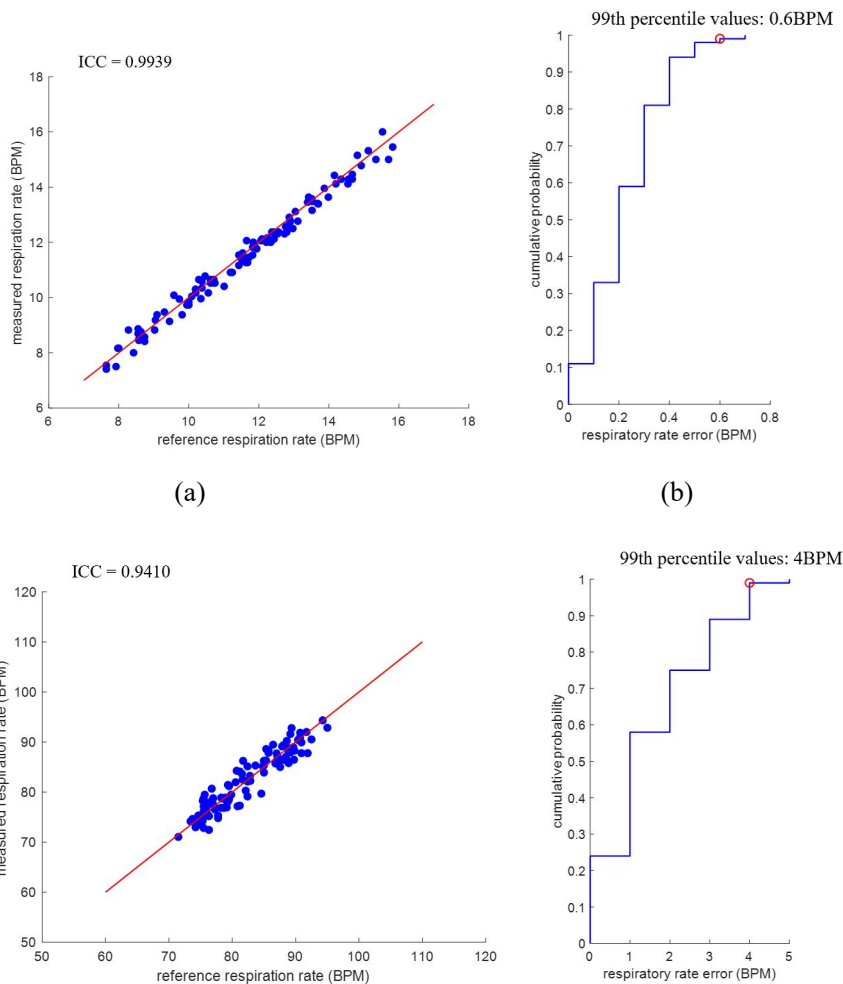
Table 4 Analysis of respiratory measurements

NUM	Type	MEAN/s	SD/s
Subject F	Radar measurement	4.52	0.38
	Reference	4.56	0.36
Subject M	Radar measurement	5.68	0.94
	Reference	5.73	0.93

Table 5 Analysis of heartbeat measurements

NUM	Type	MEAN/BPM	SD/BPM
Subject F	Radar measurement	80.71	1.67
	Reference	80.88	0.76
Subject M	Radar measurement	88.41	0.69
	Reference	86.59	1.29

To better represent the statistical properties of the accuracy of radar measurements, we collected 50 sets of data for each subject, with each set of data of 25 s duration. We then extracted One hundred RS and One hundred HS. Fig. 15 shows the Pearson correlation coefficient between the RR radar measurements and the actual values was 0.9939. The 99th percentile error of the CDF was 0.6 BPM; the Pearson correlation coefficient between the HR radar measurements and the actual values was 0.9410, and the cumulative distribution function (CDF) of the radar measurement error was 0.6 BPM. The 99% error (99th percentile error) of the cumulative distribution function (CDF) is 4BPM. The above experimental data show that the proposed method can accurately measure human respiration and heartbeat using radar.



(c)

(d)

Fig. 15 (a) and (c) are scatter plots of RR and HR, respectively, where the x-axis is the reference value, and the y-axis is the radar measurement; (b) and (d) are the cumulative distribution function (CDF) of the radar measurement error of RR and HR, respectively

V Conclusion

The simulation results show that the distortion of the algorithm extracted RS is small, with a correlation coefficient of 0.9842 with the actual signal. The distortion of the HS is slightly larger, with a correlation coefficient of 0.7176 with the actual signal. The article analyzes that the characteristics of the band-pass filter distort the HS waveform, and the correlation coefficient reaches 0.9337 without the effect of the band-pass filter. The experimental results show that the Pearson correlation coefficient between the measured and actual RR values is 0.9939, and the Pearson correlation coefficient of HR is 0.9410, which indicates that the proposed method can accurately and robustly measure human respiration and heartbeat.

The proposed method only applies to static human targets, indicating the need to eliminate random body motion (RBM). Current research has eliminated RBM by placing two radar synchronized transmit and receive signals in front of and behind the subject, with couplers, phase shifters and calibration to eliminate the ambient reflected and synchronized signals. However, this makes the system very complex. Simple and effective RBM cancellation is still an unsolved problem in respiratory heartbeat measurement, and future research will be devoted to this problem.

This paper proposes a robust method of measuring human respiration and heartbeat using millimeter wave radar. By establishing a human chest wall motion model, the tracking method of human chest wall position and the demixing method of RS, HS and noise are investigated. And it is confirmed by simulation and experiment that the method can effectively achieve accurate and robust human respiration and heartbeat measurement.

Reference

- [1] B. G. Celler and R. S. Sparks, "Home Telemonitoring of Vital Signs—Technical Challenges and Future Directions," in *IEEE Journal of Biomedical and Health Informatics*, vol. 19, no. 1, pp. 82-91, Jan. 2015.
- [2] Z. Dong et al., "A fatigue driving detection method based on Frequency Modulated Continuous Wave radar," 2021 IEEE International Conference on Consumer Electronics and Computer Engineering (ICCECE), Guangzhou, China, 2021, pp. 670-675.
- [3] L. Xie, J. Tian, H. Li and Q. Zhao, "Wireless Healthcare System for Life Detection and Vital Sign Monitoring," 2020 IEEE 91st Vehicular Technology Conference (VTC2020-Spring), Antwerp, Belgium, 2020, pp. 1-5.
- [4] J. Wang and C. Li, "A Human Tracking and Physiological Monitoring FSK Technology for Single Senior at Home Care," 2018 40th Annual International Conference of the IEEE Engineering in Medicine and Biology Society (EMBC), Honolulu, HI, USA, 2018, pp. 4432-4435.
- [5] E. Lemmer, D. Schmiech, S. Müller, A. Marnach, R. Thull and A. R. Diewald, "Development of a 24 GHz Front-End and first test measurements for Breathing and Heartbeat Monitoring inside a Cot," 2019 23rd International Conference on Applied Electromagnetics and Communications (ICECOM), Dubrovnik, Croatia, 2019, pp. 1-5.
- [6] V. P. Tran, A. A. Al-Jumaily, and S. Islam, "Doppler Radar-Based Non-Contact Health Monitoring for Obstructive Sleep Apnea Diagnosis: A Comprehensive Review," *Big Data and Cognitive Computing*, vol. 3, no. 1, p. 3, 2019.
- [7] M. Kebe, R. Gadhafi, B. Mohammad, M. Sanduleanu, H. Saleh, and M. Al-Qutayri, "Human Vital Signs Detection Methods and Potential Using Radars: A Review," *Sensors*, vol. 20, no. 5, 2020.
- [8] D. L. Abrams, "Principles of Clinical Electrocardiography," *JAMA*, vol. 249, no. 12, pp. 1642-1642, 1983.
- [9] Y. Sun and N. Thakor, "Photoplethysmography Revisited: From Contact to Noncontact, From Point to Imaging," *IEEE Transactions on Biomedical Engineering*, vol. 63, no. 3, pp. 463-477, 2016.
- [10] O. P. Singh, T. A. Howe, and M. B. Malarvili, "Real-time human respiration carbon dioxide measurement device for cardiorespiratory assessment," *Journal of Breath Research*, vol. 12, no. 2, p. 026003, 2018.
- [11] R. Scholz, B. R. Bracio, M. Brutscheck, and P. Trommler, "Non-invasive RR detection in spontaneous respiration by humidity measurement," in 2017 28th Irish Signals and Systems Conference (ISSC), 20-21 June 2017 2017, pp. 1-6.
- [12] Y. P. Huang, M. S. Young, and C. C. Tai, "Noninvasive respiratory monitoring system based on the piezoceramic transducer's pyroelectric effect," *Review of Scientific Instruments*, vol. 79, no. 3, p. 377, 2008.
- [13] N. Molinaro et al., "Wearable textile based on silver plated knitted sensor for RR monitoring," in 2018 40th Annual International Conference of the IEEE Engineering in Medicine and Biology Society (EMBC), 18-21 July 2018 2018, pp. 2865-2868.
- [14] A. Dunaeva, D. Konovalova, and V. Kostousov, "Video Analysis Methods for Remote Measurement of Respiration Characteristics and HR Variability," in 2020 Ural Symposium on Biomedical Engineering, Radioelectronics and Information Technology (USBREIT), 14-15 May 2020 2020, pp. 0171-0174.
- [15] H. Abuella and S. Ekin, "Non-Contact Vital Signs Monitoring Through Visible Light Sensing," *IEEE Sensors Journal*, vol. 20, no. 7, pp. 3859-3870, 2020.
- [16] C. Hessler, M. Abouelenien and M. Burzo, "A Non-contact Method for Extracting Heart and Respiration Rates," 2020 17th Conference on Computer and Robot Vision (CRV), 2020, pp. 1-8.
- [17] A. Wang, N. Dan, A. R. Sridhar, and S. Gollakota, "Using smart speakers to contactlessly monitor heart rhythms," *Communications Biology*, vol. 4, no. 1, p. 319, 2021.
- [18] J. Liu, Y. Chen, Y. Wang, X. Chen, J. Cheng, and J. Yang, "Monitoring Vital Signs and Postures During Sleep Using WiFi Signals," *IEEE Internet of Things Journal*, pp. 2071-2084, 2018.
- [19] M. Zakrzewski, H. Raittinen, and J. Vanhala, "Comparison of Center Estimation Algorithms for Heart and Respiration Monitoring with Microwave Doppler Radar," *IEEE Sensors Journal*, vol. 12, no. 3, pp. 627-634, 2012.
- [20] X. Yang, G. Sun, and K. Ishibashi, "Non-contact acquisition of respiration and HRs using Doppler radar with time domain peak-detection algorithm," in *Engineering in Medicine & Biology Society*, 2017.
- [21] H. Shen, Member, IEEE, X. Chen, and Y. Yang, "Respiration and Heartbeat Rates Measurement Based on Autocorrelation Using IR-UWB Radar," *Circuits and Systems II: Express Briefs, IEEE Transactions on*, vol. PP, no. 99, pp. 1-1, 2018.

- [22] Y. Xiong, S. Chen, X. Dong, Z. Peng, and W. Zhang, "Accurate Measurement in Doppler Radar Vital Sign Detection Based on Parameterized Demodulation," *IEEE Transactions on Microwave Theory and Techniques*, vol. PP, no. 11, pp. 1-10, 2017.
- [23] K. Hanifi and M. E. Karsligil, "Elderly Fall Detection With Vital Signs Monitoring Using CW Doppler Radar," *IEEE Sensors Journal*, vol. 21, no. 15, pp. 16969-16978, 2021
- [24] Y. Zhang, X. Li, R. Qi, Z. Qi, and H. Zhu, "Harmonic Multiple Loop Detection (HMLD) Algorithm for Not-Contact Vital Sign Monitoring Based on Ultra-Wideband (UWB) Radar," *IEEE Access*, vol. 8, pp. 38786-38793.
- [25] Q. Lv et al., "Doppler Vital Signs Detection in the Presence of Large-Scale Random Body Movements," *IEEE Transactions on Microwave Theory and Techniques*, vol. 66, no. 9, pp. 4261-4270, 2018.
- [26] H. Mi, Y. Nian, and B. Liu, "Noncontact heart beat signal extraction based on wavelet transform," in *2015 8th International Conference on Biomedical Engineering and Informatics (BMEI)*, 2015.
- [27] Y. Zhang, J. Li, S. Wei, F. Zhou, and D. Li, "Heartbeats Classification Using Hybrid Time-Frequency Analysis and Transfer Learning Based on ResNet," *IEEE Journal of Biomedical and Health Informatics*, vol. 25, no. 11, pp. 4175-4184, 2021.
- [28] G. W. Fang, C. Y. Huang, and C. L. Yang, "Switch-Based Low Intermediate Frequency System of a Vital Sign Radar for Simultaneous Multitarget and Multidirectional Detection," *IEEE Journal of Electromagnetics, RF and Microwaves in Medicine and Biology*, vol. 4, no. 4, pp. 265-272, 2020
- [29] K. Wang, Z. Zeng, and J. Sun, "Through-Wall Detection of the Moving Paths and Vital Signs of Human Beings," *IEEE Geoscience and Remote Sensing Letters*, vol. 16, no. 5, pp. 717-721, 2019
- [30] J. Li, L. Liu, Z. Zeng, and F. Liu, "Advanced Signal Processing for Vital Sign Extraction With Applications in UWB Radar Detection of Trapped Victims in Complex Environments," *IEEE Journal of Selected Topics in Applied Earth Observations and Remote Sensing*, vol. 7, no. 3, pp. 783-791, 2014.
- [31] H. Zhao, H. Hong, L. Sun, Y. Li, C. Li, and X. Zhu, "Noncontact Physiological Dynamics Detection Using Low-power Digital-IF Doppler Radar," *IEEE Transactions on Instrumentation and Measurement*, vol. 66, no. 7, pp. 1780-1788, 2017.
- [32] J. Tu and J. Lin, "Respiration harmonics cancellation for Accurate HR measurement in non-contact vital sign detection," *IEEE MTT-S International Microwave Symposium digest. IEEE MTT-S International Microwave Symposium*, pp. 1-3, 2013.
- [33] Y. Xiong, Z. Peng, C. Gu, S. Li, D. Wang, and W. Zhang, "Differential Enhancement Method for Robust and Accurate HR Monitoring via Microwave Vital Sign Sensing," *IEEE Transactions on Instrumentation and Measurement*, vol. 69, no. 9, pp. 7108-7118, 2020.
- [34] R. Ambarini, A. A. Pramudita, E. Ali, and A. D. Setiawan, "Single-Tone Doppler Radar System for Human Respiratory Monitoring," in *2018 5th International Conference on Electrical Engineering, Computer Science and Informatics (EECSI)*, 16-18 Oct. 2018 2018, pp. 571-575.
- [35] W. Xia, Y. Li, and S. Dong, "Radar-Based High-Accuracy Cardiac Activity Sensing," *IEEE Transactions on Instrumentation and Measurement*, vol. PP, no. 99, pp. 1-1, 2021.
- [36] L. Lu, X. Ma, X. Fan, R. Hao, L. Li, and X. Fan, "Vibrating Clutter Interference Removal Technique in FMCW Radar for Mechanical Vibration and Vital Sign Detection," in *2021 IEEE International Symposium on Radio-Frequency Integration Technology (RFIT)*, 25-27 Aug. 2021 2021, pp. 1-3
- [37] I. V. Semernik, A. V. Dem'Yanenko, and O. E. Semernik, "Three-dimensional Electrodynamical Model of the Human Chest," in *2020 IEEE Conference of Russian Young Researchers in Electrical and Electronic Engineering (EIconRus)*, 2020.
- [38] M. Jankiraman, *FMCW Radar Design*. London, U.K.: Artech House, 2018.
- [39] P. Kumar and G. S. Ranganath, "Geometrical theory of diffraction," *Pramana*, vol. 37, no. 6, pp. 457-488, 1991.
- [40] G. Yan, Q. Pan, and K. Yang, "Research on a new Gaussian self-adaptive smoothing algorithm in image processing," in *VLSI Design and Video Technology*, 2005. *Proceedings of 2005 IEEE International Workshop on*, 2005.
- [41] P. Luo, W. Zhang. *Random Signal Analysis and Processing*[M]. Tsinghua University Press, 2006.